Single-isocenter stereotactic radiosurgery for multiple brain metastases: Impact of patient misalignments on target coverage in non-coplanar treatments

Michael Martin Eder[1,2,4], **Michael Reiner**[1], **Christian Heinz**[1], **Sylvia Garny**[1], **Philipp Freislederer**[1], **Guillaume Landry**[1,2], **Maximilian Niyazi**[1,3], **Claus Belka**[1,3], **Marco Riboldi**[1,*]

[1] Department of Radiation Oncology, University Hospital, LMU Munich, Munich, Germany
[2] Department of Medical Physics, Ludwig-Maximilians University, Garching, Germany
[3] German Cancer Consortium (DKTK), Partner Site Munich, Munich, Germany

Received 6 September 2021; accepted 14 February 2022

Abstract

Frameless single-isocenter non-coplanar stereotactic radiosurgery (SRS) for patients with multiple brain metastases is a treatment at high geometrical complexity. The goal of this study is to analyze the dosimetric impact of non-coplanar image guidance with stereoscopic X-ray imaging. Such an analysis is meant to provide insights on the adequacy of safety margins, and to evaluate the benefit of imaging at non-coplanar configurations.

The ExacTrac® (ET) system (Brainlab AG, Munich, Germany) was used for stereoscopic X-ray imaging in frameless single-isocenter non-coplanar SRS for multiple brain metastases. Sub-millimeter precision was found for the ET-based pre-treatment setup, whereas a degradation was noted for non-coplanar treatment angles. Misalignments without intra-fractional positioning corrections were reconstructed in 6 degrees of freedom (DoF) to resemble the situation without non-coplanar image guidance.

Dose recalculation in 20 SRS patients with applied positioning corrections did not reveal any significant differences in $D_{98\%}$ for 75 planning target volumes (PTVs) and gross tumor volumes (GTVs). For recalculation without applied positioning corrections, significant differences ($p < 0.05$) were reported in $D_{98\%}$ for both PTVs and GTVs, with stronger effects for small PTV volumes. A worst-case analysis at increasing translational and rotational misalignment revealed that dosimetric changes are a complex function of the combination thereof.

This study highlighted the important role of positioning correction with ET at non-coplanar configurations in frameless single-isocenter non-coplanar SRS for patients with multiple brain metastases. Uncorrected patient misalignments at non-coplanar couch angles were linked to a significant loss of PTV coverage, with effects varying according to the combination of single DoF and PTV geometrical properties.

Keywords: Stereotactic radiosurgery, Multiple brain metastases, Single-isocenter, Non-coplanar, Patient positioning, Stereoscopic X-ray imaging

* Corresponding author: Marco Riboldi, Department of Radiation Oncology, University Hospital, LMU Munich, Munich, Germany.
E-mail addresses: mi.eder@protonmail.com (M.M. Eder), michael.reiner@med.uni-muenchen.de (M. Reiner), christian.heinz@med.uni-muenchen.de (C. Heinz), sylvia.garny@med.uni-muenchen.de (S. Garny), philipp.freislederer@med.uni-muenchen.de (P. Freislederer), guillaume.landry@med.uni-muenchen.de (G. Landry), maximilian.niyazi@med.uni-muenchen.de (M. Niyazi), claus.belka@med.uni-muenchen.de (C. Belka), marco.riboldi@physik.uni-muenchen.de (M. Riboldi).
[4] Present address: Brainlab AG, Munich, Germany.

Z Med Phys **32** (2022) 296–311
https://doi.org/10.1016/j.zemedi.2022.02.005
www.elsevier.com/locate/zemedi

1 Introduction

Stereotactic radiosurgery (SRS) for multiple brain metastases delivered with a conventional linear accelerator (LINAC) is challenging from a technical point of view, in terms of treatment planning and treatment delivery [1]. As a category, multi-isocenter techniques are characterized by using an individual isocenter for every metastasis. This allows treating each metastasis on a unique arc, so that highly conformal delivery techniques like dynamic conformal arc therapy (DCAT) can be employed to achieve a steep dose gradient at the borders of the lesion. Limitations exist for the dose gradient outside the arc plane, which may require delivery of multiple arcs. DCAT uses the LINAC's multileaf collimator (MLC) to dynamically conform the radiation field to the shape of the target volume along an arc's path [2]. However, multi-isocenter techniques are time-consuming to employ for patients with multiple brain metastases, since patient setup procedures need to be repeated for each lesion.

To make treatments of multiple metastases more efficient, single-isocenter techniques using volumetric modulated arc therapy (VMAT) or DCAT were established [3,4]. Such techniques potentially enable the irradiation of multiple metastases with a single arc, thus providing a significant additional speed-up in the irradiation procedure. Despite the restriction to a single isocenter, these treatment delivery techniques performed comparably in terms of outcome to their multi-isocentric counterparts [5,6]. To exploit multiple beam directions for both delivery techniques, the inclusion of various treatment couch angles is possible. This is commonly referred to as non-coplanar treatment delivery. For VMAT, a study conducted by Clark et al. [3] revealed improvements in planning target volume (PTV) conformity as well as sharper dose gradients, especially in the case of closely spaced lesions, for non-coplanar VMAT compared to its coplanar counterpart. For application of DCAT in the treatment of multiple brain metastases with a single-isocenter, a specialized form of the technique was proposed by Huang et al. [4]. A commercially available derivative of this DCAT technique was evaluated against single-isocenter VMAT by Gevaert et al. [5] and Hofmaier et al. [7]. Both groups reported an increase in the treatment efficiency and healthy brain sparing for the novel DCAT, while maintaining a similar PTV conformity to the VMAT plan.

In general, the single-isocenter SRS approach requires closer attention to accurate patient positioning, since rotational uncertainties have a growing influence on the target coverage for lesions with increasing distances from the isocenter [8–12]. For frameless multiple-target single-isocenter non-coplanar SRS it is recommended to define dedicated margins around the metastases and, in combination with image-guided radiotherapy (IGRT), to monitor and correct patient misalignments [9]. In addition, accurate radiation isocentricity between gantry, collimator and couch rotation must be guaranteed [13]. A wide variety of IGRT devices are available, including surface surrogates, cone-beam computed tomography (CBCT), and stereoscopic X-ray imaging. These can be subdivided into technologies compatible with couch rotations (e.g. surface surrogates, stereoscopic X-ray imaging) and not compatible ones (e.g. CBCT). Stereoscopic X-ray imaging consists of a combination of two X-ray tubes and two electronic portal imaging devices (EPIDs) mounted on the treatment room's floor or ceiling. The room-fixed setup allows imaging at non-coplanar configurations, however the LINAC's gantry may obstruct the X-ray beam in certain cases, so that only a single image can be acquired. The central idea is based on a co-registration of both X-ray images with the corresponding digitally reconstructed radiographs (DRRs), which are precalculated from the planning X-ray computed tomography (CT) scan, to determine patient misalignment in 6 degrees of freedom (DoF). Such imaging technologies are favored for non-coplanar SRS, because they allow positioning verification at all possible couch angles. This is particularly beneficial for compensating mechanical inaccuracies in the isocentric couch rotation, leading to an accuracy which is compatible with SRS requirements [14–18]. Open questions remain concerning the effective dosimetric benefit of imaging-based corrections at multiple angles, which imply a longer setup procedure [19].

For conventional C-arm LINACs, the commercially available stereoscopic X-ray imaging system is ET (Brainlab AG, Munich, Germany). With respect to frameless cranial SRS, the system was proven to be accurate for patient setup at coplanar and non-coplanar configurations in several clinical studies [19–22]. ET offers a setup accuracy comparable to kilovoltage CBCT [16,23] and an imaging dose for a stereoscopic acquisition which is about a factor 100 less than a complete kilovoltage CBCT scan [24].

The aim of this work is to quantify and compare the dosimetric effects of corrected and uncorrected patient misalignments in single-isocenter non-coplanar DCAT SRS for patients with multiple brain metastases. We analyze data from patients treated at conventional LINACs, with the possibility to image and correct at each couch angle. Our results are meant to serve as a benchmark on the significance of non-coplanar image guidance for this specialized form of radiotherapy (RT), as a function of target size, distance from the isocenter, and magnitude of residual misalignments.

2 Material and methods

2.1 Image acquisition

A total of 38 patients, who were treated for multiple brain metastases with single-isocenter non-coplanar SRS, were included in this study. Each of them underwent a pretreatment magnetic resonance imaging (MRI) scan; images were acquired with a magnetization prepared rapid gradient echo (MPRAGE) sequence with contrast agent and an axial slice

increment of 1 mm. Following the institution's rationale, the time span between MRI scan and planning CT scan was kept as short as possible and was in all cases strictly within 1 week. Before the CT scan was performed, patients were immobilized using a double layer thermoplastic mask in combination with a compatible couch extension (iCast Head Double, IT-V, Innsbruck, Austria). A contrast agent was injected, if not contraindicated, to enhance subsequent co-registration with the MRI scans. Comparable to the MRI, the CT scan was acquired as well with a 1 mm axial slice increment.

2.2 Treatment planning

The treatment planning system Elements® Multiple Brain Mets SRS (MBMSRS) v1.5 by Brainlab AG (Munich, Germany) was used to create single-isocenter non-coplanar SRS treatment plans. MRI and CT scans were co-registered using the software's automatic rigid image fusion. The result of the fusion process was visually inspected and, if necessary, manually adjusted. Segmentation of relevant organs at risk (OARs) was achieved by automatic segmentation with the results reviewed by a radiation oncologist. OARs included the brainstem, optic nerves, chiasm, hippocampus and the whole brain. Contouring of the visible metastases was performed manually while simultaneously taking axial, coronal, and sagittal slices into account. For the definition of the PTVs a 1 mm isotropic safety margin was used, assuming setup correction performed at each couch angle [25]. Prescription doses were set according to national [26] and international guidelines [27] and ranged from 15 Gy to 20 Gy (mean ± SD = 18.9 Gy ± 1.0 Gy) with all treatments performed in a single fraction. The prescription isodose lines were forced to cover 98% of their respective PTV. Prescription isodose level values were within 72–86%. The treatment plans were generated within MBMSRS using a specialized DCAT delivery technique [7]. Treatment planning relied on templates, which contained 5 to 6 different couch angles (couch angle 0° was always used) and a minimum collimator angle of 4° to reduce the dosimetric impact of interleaf radiation leakage. The templates and thus the used angles were chosen on a patient-per-patient basis. Moreover, the position of the treatment isocenter was automatically determined by MBMSRS as the non-weighted geometrical average of the PTVs' center of mass coordinates. Dose calculation was performed using a pencil beam (PB) algorithm. The finalized treatment plans were reviewed by a senior radiation oncologist together with a senior medical physicist. If the plan review did not meet the clinical expectations with respect to prescription and OAR sparing, the plan optimization was relaunched with a different template or the prescription doses were updated accordingly.

2.3 Treatment delivery

Treatment delivery started not later than 10 days after the pre-treatment MRI scan was acquired. All treatments were performed on a Versa HD™ LINAC equipped with Agility™ MLC featuring 80 leaf pairs with 5 mm leaf width at isocenter (both Elekta AB, Stockholm, Sweden) at 6 MV photon radiation under stereoscopic X-ray image guidance with ET v6.5.

At first, the patient was manually positioned based on reference marks and treatment room lasers on a HexaPOD™ evo RT System 6D robotic couch (Elekta AB, Stockholm, Sweden) at treatment couch angle 0°. For infrared based (IR) monitoring of the couch position using ET, a dedicated reference frame was attached to the couch top on a patient-individual basis.

Following manual setup, a pair of oblique X-ray images was acquired with ET. The resulting 6D patient misalignment reported by the system was corrected using the robotic couch (Figure 1). After that, a second acquisition was performed to verify correct positioning of the patient. If the residual misalignment was smaller than 0.7 mm in each translational direction and 0.5° about each axis, the patient was considered adequately positioned. Otherwise, couch corrections had to be repeated until the tolerances were eventually met (Figure 1). For simplicity, the first acquisition after manual setup and the final setup acquisition reporting residual 6D misalignment beneath tolerance are referred to as X-ray setup correction (XSC) and X-ray setup verification (XSV), respectively (Figure 1).

Following the positioning routine, the first arc at couch angle 0° was treated. Upon completion, the treatment couch was rotated towards the highest positive treatment couch angle. Subsequently, X-ray verification (XV) was performed with ET. If the reported 6D misalignment was below the tolerance values, treatment of the corresponding arc was directly performed. If not, couch correction was carried out without further verification of potential post-correction misalignment. For certain couch angles the IR monitoring system was obstructed. In these cases treatment had to be carried out without XV, due to software restrictions. This workflow was repeated for each non-coplanar arc from the treatment plan.

2.4 ExacTrac coordinate system

Understanding the installation-specific ExacTrac coordinate system (ECS) is crucial, for the simulation of patient-based misalignment at each treatment couch angle. The coordinate system's origin is declared as the imaging isocenter, which was calibrated at our installation such that it minimizes the LINAC's mechanical inaccuracies over all 4 cardinal gantry angles (i.e. 0°, 90°, 180°, and 270°). As a result, it coincides with the LINAC's radiation isocenter. Its geometrical stability and calibration accuracy are checked on a regular basis using established quality assurance (QA) procedures.

The 6 DoF in patient misalignment are reported by ET in the ECS as offsets with respect to the ideal couch position. In

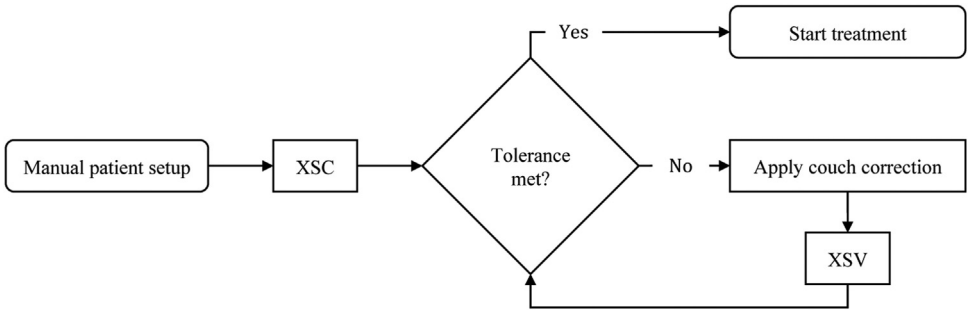

Figure 1. Flowchart of the X-ray based setup workflow performed for each patient with the couch at 0°.

the case of head-first supine positioning of the patient, positive translational offsets in all three spatial directions correspond to the patient's treatment isocenter being positioned too far patient left, superior, and anterior with respect to the imaging isocenter. The 3 rotational DoF are called pitch, roll, and yaw and used to describe a tilting of the patient about its treatment isocenter. For our installation, they denote a left-handed rotation about the patient right-left (RL) axis, left-handed rotation about the inferior–superior (IS) axis, and right-handed rotation about the posterior–anterior (PA) axis, respectively.

2.5 Treatment scenarios

Two different treatment scenarios were simulated based on the clinically reported patient misalignments (Figure 2). Such scenarios, along with systematic shifts in 6 DoF, were considered for dose recalculation, as detailed in Section 2.7.

2.5.1 *Applied correction scenario*

In the applied correction scenario (AC), 6 DoF residuals following XV were used for dosimetric calculations (Figure 2a). Couch angles where XV was not feasible, or where additional setup corrections were applied due to unmet tolerance levels, were treated as if perfect setup (i.e. null 6 DoF residuals) was achieved. This is consistent with the fact that no experimental data were available to quantify the residual misalignment in this case, and that any potential misalignment could always be corrected, if necessary.

2.5.2 *No correction scenario*

As corrections at a given couch angle were clinically applied, the subsequently reported patient misalignments were all intrinsically affected by the correction itself. In order to simulate the no correction scenario (NC), a specific procedure was implemented to reconstruct the raw misalignments (Figure 2b). Relative offsets in 6 DoF were calculated from the misalignments reported in the previous acquisition, according to the following formula:

$$\mathrm{DoF}_{i,\mathrm{rel}} = \begin{cases} 0 & \text{if XV not feasible due to obstructed view,} \\ \mathrm{DoF}_i & \text{if correction followed previous acquisition,} \\ \mathrm{DoF}_i - \mathrm{DoF}_{i-1} & \text{otherwise.} \end{cases} \tag{1}$$

for $i > 0$, where $\mathrm{DoF}_{0,\mathrm{rel}}$ corresponds to the 6 DoF reported by XSV. Consistently with the AC scenario, couch angles where XV was not feasible were treated as if perfect setup was achieved, thus assuming no relative misalignment to the previous acquisition. The raw misalignments were then reconstructed by a cumulative summation of all relative offsets up to couch rotation angle k:

$$\mathrm{DoF}_{k,\mathrm{raw}} = \sum_{i=0}^{k} \mathrm{DoF}_{i,\mathrm{rel}} \tag{2}$$

We finally applied the calculated raw misalignments $\mathrm{DoF}_{k,\mathrm{raw}}$ to simulate the NC scenario.

2.6 Geometrical risk assessment of patient misalignment

The risk of loss in PTV coverage was quantified geometrically for every patient, as a function of the reported misalignments at each couch angle. The risk was calculated in terms of geometrical overlap between the treatment planning PTV and the PTV transformed (i.e. shifted and rotated) according to the NC scenario. The procedure to classify each case in terms of geometrical risk of coverage loss was as follows:

- Exported patient's structure sets were transformed into a binary image in the same frame of reference of the treatment planning CT, relying on the open source tool *plastimatch* (v1.7.3) [28].
- At each couch angle, all patient's associated PTVs were rigidly transformed according to the corresponding 6 DoF from the NC scenario about the treatment isocenter

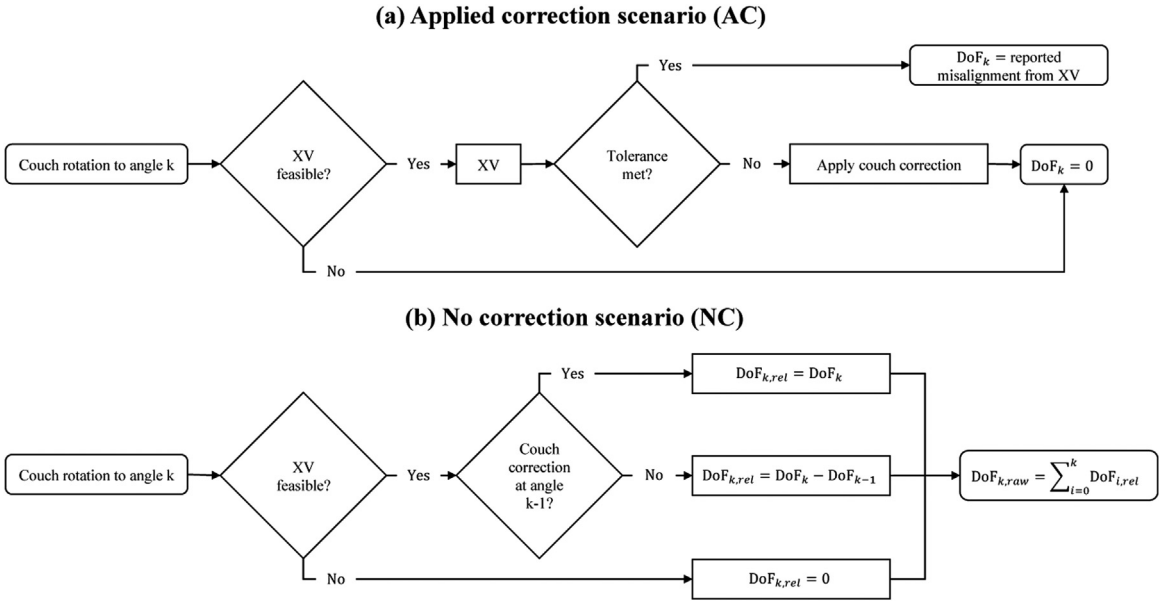

Figure 2. Flowchart of the simulated AC (a) and NC (b) scenarios for the treatment couch positioned at couch angle *k*.

(considering the ET coordinate system) and rebinarized using linear interpolation and a 50% thresholding.
- The Dice-Sørensen coefficients (DSCs) [29,30] were calculated between the initial PTVs and their transformed versions.

As a result, exact geometrical overlap between both PTVs is given by a DSC equal to 1, corresponding to a null 6 DoF transformation. Conversely, uncompensated misalignments in the NC scenario are supposed to lead to reduced DSC values, thus indicating higher risk of PTV coverage loss.

2.7 Dose recalculation under patient misalignment

The aim of dose recalculation under patient misalignment was to dosimetrically study the effects that patient-individual positioning errors have on the corresponding planned dose distribution. This study considered 20 patients treated with single-isocenter non-coplanar SRS for multiple brain metastases, selected according to the geometrical risk assessment, as described in Section 2.6. The patients at higher geometrical risk were chosen: Table 1 lists details on the analyzed patient cohort.

For the purpose of dose recalculation, a dedicated prototype of MBMSRS v2.0 was developed in cooperation with the vendor. It is capable of transforming the internal patient model including the orientation of the model-fixed dose calculation grid according to patient misalignments in 6 DoF under a certain treatment couch angle. As a direct result of the chosen implementation, no additional interpolation of the CT image nor dose grid was required, thus avoiding potential uncertainties to the results introduced by such procedures. As the PB algorithm was subject to refinements for MBMSRS v2.0, the clinically accepted treatment plans were anonymized and exported from MBMSRS v1.5 and recalculated without any patient misalignment within the prototype. The resulting dose distribution then served as a reference baseline for comparison purposes. Comparably to the treatment planning workflow, the recalculation was performed with the PB algorithm in a 1 mm uniform dose grid.

The dosimetric analysis was carried out using an in-house Python script. The following scenarios were simulated:

- The AC treatment scenario (Section 2.5.1),
- the NC treatment scenario (Section 2.5.2),
- and systematic misalignments in 6 DoF with respect to the treatment plan (Section 2.7.1).

In the first step, the patient's structure set was exported from MBMSRS and transformed into a binary image according to the dose grid's geometry. After that, dose-volume histogram (DVH) parameters such as D_{mean}, $D_{2\%}$, and $D_{98\%}$ were calculated for all gross tumor volumes (GTVs), PTVs and OARs in each scenario's corresponding dose distribution. Relative DVH parameters ΔD_{mean}, $\Delta D_{2\%}$, and $\Delta D_{98\%}$ were calculated as well. They are defined as the absolute DVH parameter for a given scenario minus the one obtained for the reference baseline. In addition, a dedicated relative analysis parameter – the coverage change to reference (CCR) – was established to quantify the percentage of coverage potentially lost or gained when compared to the planned dose distribution. For each scenario's dose distribution it is calculated as

$$\text{CCR} = 98\% - V_{\text{TV}}\left(D_{98\%}^{\text{ref}}\right) \tag{3}$$

Table 1
Overview of the analyzed patient cohort.

Total number of analyzed patients	20	Female: 9, Male: 11
Median age at SRS	63 years	Range: 33 years to 74 years
Total number of treated metastases	75	
Median number of treated metastases per patient	3	Range: 2 to 10
Median prescription isodose	19 Gy	Range: 15 Gy to 20 Gy
Median PTV volume	0.28 cm^3	Range: 0.05 cm^3 to 6.13 cm^3
Median GTV volume	0.11 cm^3	Range: 0.01 cm^3 to 4.15 cm^3
Median PTV to isocenter offset	46.6 mm	Range: 6.9 mm to 79.5 mm
Median number of couch angles per patient	6	Range: 5 to 6
Total number of verified couch angles	86	Corrected: 24 (28%) Accepted: 62 (72%)
Total number of unverified couch angles	9	At treatment couch angles: 270°, 280°, 300°, and 315°

where $V_{TV}(D^{ref}_{98\%})$ denotes the percentage of the target volume (i.e. GTV or PTV) covered by the $D_{98\%}$ dose level obtained from the reference distribution. Thus, a negative or positive CCR indicates an increase or decrease of coverage in the corresponding scenario, respectively. Furthermore, geometrical properties such as the target structures' volumes and isocentric offsets from their centers of mass were calculated as well using the in-house Python script.

2.7.1 Systematic misalignments

The dose cubes were recalculated under multiple 6 DoF transformations, mimicking patient misalignment at pre-defined magnitudes. Systematic translations of 0.5 mm, 0.7 mm, 1.0 mm, 1.5 mm, 2.0 mm, and 2.5 mm as well as rotations of 0.5°, 1°, 1.5°, 2°, and 2.5° were applied individually and simultaneously in the corresponding directions. In summary, a total of 58 dose recalculations and dosimetric impact evaluations were performed.

2.7.2 Clinical misalignments

For studying the dosimetric impact of patient misalignment, each set of arcs belonging to a single treatment couch angle had to be calculated individually by taking the corresponding 6 DoF for each scenario into account. As a result, a partial dose distribution for that specific couch angle was acquired. The total dose distribution for the complete non-coplanar SRS treatment was finally calculated by summing up all individual partial dose distributions using an in-house Python script. As all partial dose distributions shared the same geometry, no interpolation was required to restore the total dose distribution for each scenario.

Non-parametric Friedman tests [31] were conducted to check for statistically significant differences in the absolute DVH parameters across both scenarios (i.e. AC and NC) and the reference baseline. For a significant p-value ($p < 0.05$) reported by the Friedman test, a non-parametric post-hoc analysis in the form of a Nemenyi test [32,33] was carried out to determine which of the two-sided comparisons actually reported significant differences. The statistical tests were performed using their implementation in the Python modules *SciPy* (v1.1.0) as well as *scikit-posthocs* (v0.6.5).

3 Results

3.1 Analysis of patient misalignment

The patient misalignment reported by ET was retrospectively exported from the ET treatment console for the treatment sessions of the 38 patients included in this study. The analyzed data featured a total of 227 XVs, split up in 38 acquisitions each for XSC and XSV. The remaining 151 acquisitions were linked to non-coplanar positioning verifications.

A number of 4 to 5 non-coplanar XVs was reported for 27 treatment sessions, which corresponds to the selection of 5 to 6 different treatment couch angles with couch angle 0° being used in each plan. Discrepancies were found for 11 patients with 3 or less non-coplanar XVs. These were caused by two issues. Firstly, XVs were sometimes inhibited for certain couch angles due to an obstructed view of the IR reference frame. Secondly, as the treatment may have been interrupted for whatever reason, the patient had to be repositioned at couch angle 0°. Thereby a new treatment session was created which only featured the residual arcs that where not irradiated before the interruption took place. Such secondary sessions were purposely excluded from the analyzed data. From the 151 non-coplanar XVs a total number of 40 acquisitions (26.5%) were found with at least one DoF being out of tolerance. From these 40, 34 were further corrected, thus resulting in 6 out of tolerance acquisitions where no further correction was performed (visible as outliers for the AC scenario in Figure 4). This discrepancy is explained by the fact that the final decision on whether the misalignment should be corrected was taken by the treating physician on a patient-individual basis.

3.1.1 Patient setup

An analysis of patient misalignment reported by XSC and XSV was conducted with the aim to quantify the setup

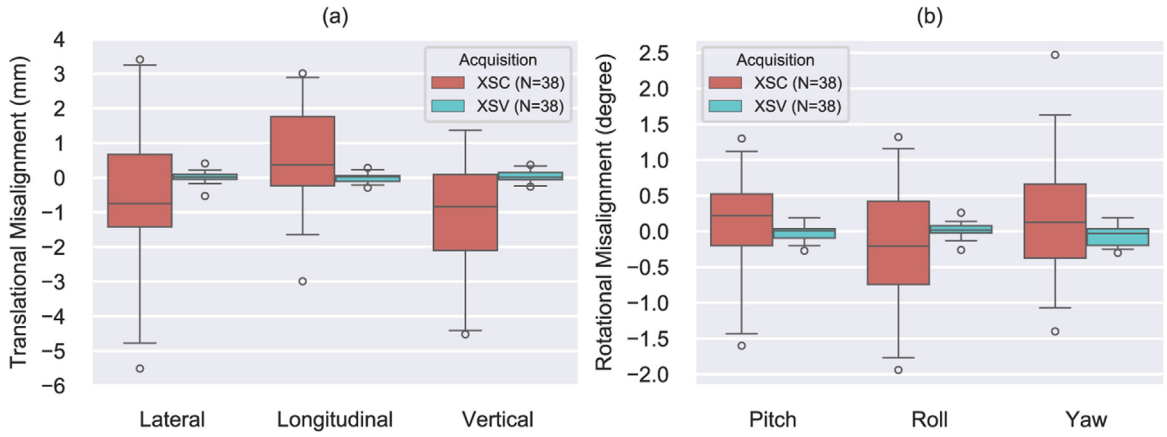

Figure 3. Residual translational (a) and rotational (b) misalignment at the stage of patient setup as reported by ET XV. XSC refers to the 6 DoF from the acquisition performed after manual prepositioning based on treatment room lasers, whereas XSV indicates the residual misalignment reported from the acquisition following treatment couch correction. The boxes span from the 25th percentile to the 75th percentile thus displaying the IQR. Their lower and upper whiskers indicate the range between the 2.5th percentile and 97.5th percentile. Values outside this 95% CI are considered outliers.

Table 2
Statistical quantities (i.e. Median, Q_1: 1st quartile, Q_3: 3rd quartile, and SD) for the 6 DoF in patient misalignment at the stage of manual (XSC) and ET-based (XSV) patient setup as reported by ET XV.

	lat (mm)		long (mm)		vert (mm)		pitch (°)		roll (°)		yaw (°)	
	XSC	XSV	XSC	XSV	XSC	XSV	XSC	XSV	XSC	XSV	XSC	XSV
Median	−0.8	0.0	0.4	0.0	−0.8	0.0	0.2	0.0	−0.2	0.0	0.1	0.0
Q_1	−1.4	−0.1	−0.2	−0.1	−2.1	−0.1	−0.2	−0.1	−0.7	0.0	−0.4	−0.2
Q_3	0.7	0.1	1.8	0.1	0.1	0.2	0.5	0.0	0.4	0.1	0.7	0.0
SD	2.0	0.2	1.3	0.1	1.5	0.2	0.7	0.1	0.8	0.1	0.8	0.1

accuracy of ET. The reported translational and rotational DoF for both acquisition types are visualized in Figure 3. Statistical quantities complementing the plots are found in Table 2. When comparing the misalignments between XSC and XSV, a substantial decrease of the interquartile range (IQR) Q_3–Q_1 was noted for all 6 DoF when performing ET-based setup after manual prepositioning, as expected. Additionally, median values were closer to zero in the XSV compared to the ones reported by XSC. Furthermore, a decline in the standard deviation (SD) was found for all translational and rotational DoF.

3.1.2 Non-coplanar patient misalignment

To quantify the 6 DoF in non-coplanar patient misalignment, the 151 remaining acquisitions were analyzed for the AC and NC scenario. The results are plotted in Figure 4.

From there it is apparent that the IQR and the median values are very much comparable between both scenarios. However, stronger differences were noted in the 95% CI and in the outliers. They appeared to be more prominent along the lateral and longitudinal direction for translational misalignment as well as in pitch and yaw for rotational misalignment. In general, absolute misalignments were reported with higher magnitude in the NC scenario.

The number of DoF reported out of tolerance increased from 6 to 64 when comparing the AC to the NC scenario. Consequently, the data variability is higher in the NC scenario. Undoubtedly, the strongest effects were reported for the outliers. For example, the maximum yaw misalignment went up from 0.6° to 1.2° and the minimum pitch angle decreased from −0.4° to −1.4°.

3.2 Geometrical risk assessment of patient misalignments

A total of 130 PTVs and 181 treatment couch angles were included in the DSC calculations: as a result, a total of 651 DSCs were reported. They are scattered against their corresponding PTV's volume V_{PTV} and its distance to the treatment isocenter d_{iso} in Figure 5a and b, respectively. The associated correlation was determined by Spearman's rank correlation coefficient ρ [34]. For V_{PTV} it was reported weak with $\rho = 0.2$ ($p_\rho = 4.4 \times 10^{-7}$) and even weaker with $\rho = -0.1$ ($p_\rho = 1.5 \times 10^{-1}$) for d_{iso}.

The DSCs for the translational DoF are found in Figure 5c, whereas Figure 5d highlights their relation with respect to the rotational DoF. The correlation between DSC and

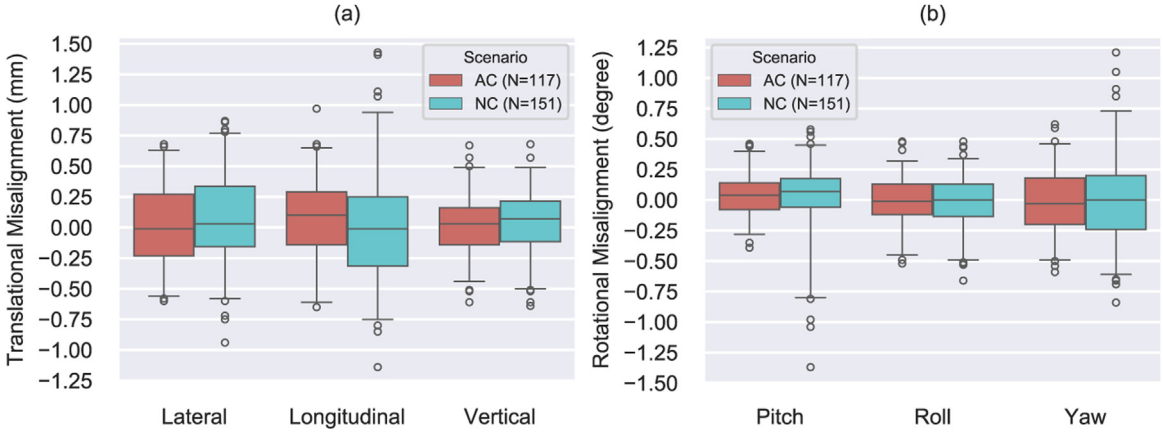

Figure 4. Translational (a) and rotational (b) misalignment at non-coplanar treatment couch angles as reported by ET XV for the AC and NC scenario. The boxes span from the 25th percentile to the 75th percentile thus displaying the IQR. Their lower and upper whiskers indicate the range between the 2.5th percentile and 97.5th percentile. Values outside this 95% CI are considered outliers. Data from the 34 acquisitions followed by a couch correction are not included in the boxplot of the AC scenario, to avoid bias in the distribution due to multiple zeros.

translational DoF was strong with $\rho = -0.8$ ($p_\rho = 5.2 \times 10^{-147}$). For the rotational DoF it was weaker with $\rho = -0.4$ ($p_\rho = 4.7 \times 10^{-28}$). In addition, a multi-parameter scatterplot is given in Figure 5e. It indicates the effect that a patient misalignment in all its combined 6 DoF has onto the DSC. The combined 6 DoF is defined as the sum of the vector lengths of the corresponding translational and rotational misalignment, expressed in millimeter and degrees, respectively. The offset from the treatment isocenter d_{iso} is color-coded and the absolute PTV volume V_{PTV} is represented by the size of the markers. To allow better visualization, the plot only features the 620 DSCs corresponding to the 123 PTVs where V_{PTV} is smaller than 4 cm^3.

Furthermore, a ranking of the patients was conducted based on the minimal DSC that was reported for each patient-based PTV and misalignment combination. The five patients with the highest risk are given in Table 3 together with the patient having the least risk. A total number of 13 translational and 10 rotational DoF were out of tolerance for the PTV and misalignment combinations that led to the minimal DSCs. Statistical analysis was performed for these combinations. V_{PTV} ranged from 0.05 cm^3 to 5.56 cm^3 (mean ± SD = 0.56 cm^3 ± 0.97 cm^3) and d_{iso} was contained within 7.1 mm and 74.6 mm (mean ± SD = 44.5 mm ± 19.4 mm). Furthermore, DSCs were reported from 0.54 to 0.96 (mean ± SD = 0.79 ± 0.10).

3.3 Dosimetric impact of systematic misalignments

After verification of the geometrical impact of patient misalignment, the corresponding dosimetric impact was studied for the worst-case patient. The selected patient was a 72-year-old woman diagnosed with 5 brain metastases. The patient did undergo single-isocenter non-coplanar SRS under ET guidance with a total of six couch angles (i.e. 0°, 30°, 60°, 285°, 315°, and 345°). The treatment plan featured a total of 5950 monitor units (MUs). Each PTV was prescribed to 19 Gy covering 98% of its corresponding volume. Additional geometrical information on the GTVs and PTVs is found in Table 4.

Statistical data of a few selected treatment planning parameters for PTVs is given in Table 5. The 58 dose calculations for each of the 5 PTVs (as described in Section 2.7.1) led to a total of 290 simulations. As 5 out of these 290 corresponded to null misalignments, 285 recalculations were considered in total for non-zero misalignments. These were split into 100 translations, 100 rotations and 85 combinations (Table 5). For $\Delta D_{2\%}$ the mean values were for all three groups zero or below and the minimum values down to −3.3 Gy for the translational errors, meaning that the hottest 2% of the volume received in general less dose than in the reference distribution. The same effect but with stronger characteristic was noted for $\Delta D_{98\%}$. Thus, the dose covering 98% of the PTVs was substantially reduced under present misalignments. A close relative of this parameter is the CCR given in (3). The corresponding means were at lowest with 14.8% for rotational errors. They showed an increase to 27.4% and 38.3% for pure translations and combinations, respectively. An appropriate estimator of the change in overall tendency of a PTV's DVH is given by ΔD_{mean}. Negative mean values were reported for this parameter in all three groups. Therefore, the DVH curves tended to be shifted to lower absolute dose values.

The $\Delta D_{98\%}$ parameter is visualized with respect to the individual PTVs in Figure 6. The parameter was decreasing systematically for increasing translational misalignments (Figure 6a). Small target volumes such as PTV 1, PTV 4, and PTV 5 turned out to be more strongly affected by the positioning errors in translation. Furthermore, a continuous reduction of $\Delta D_{98\%}$ was noted for growing rotational misalignments (Figure 6b). However, the overall magnitude of $\Delta D_{98\%}$ was

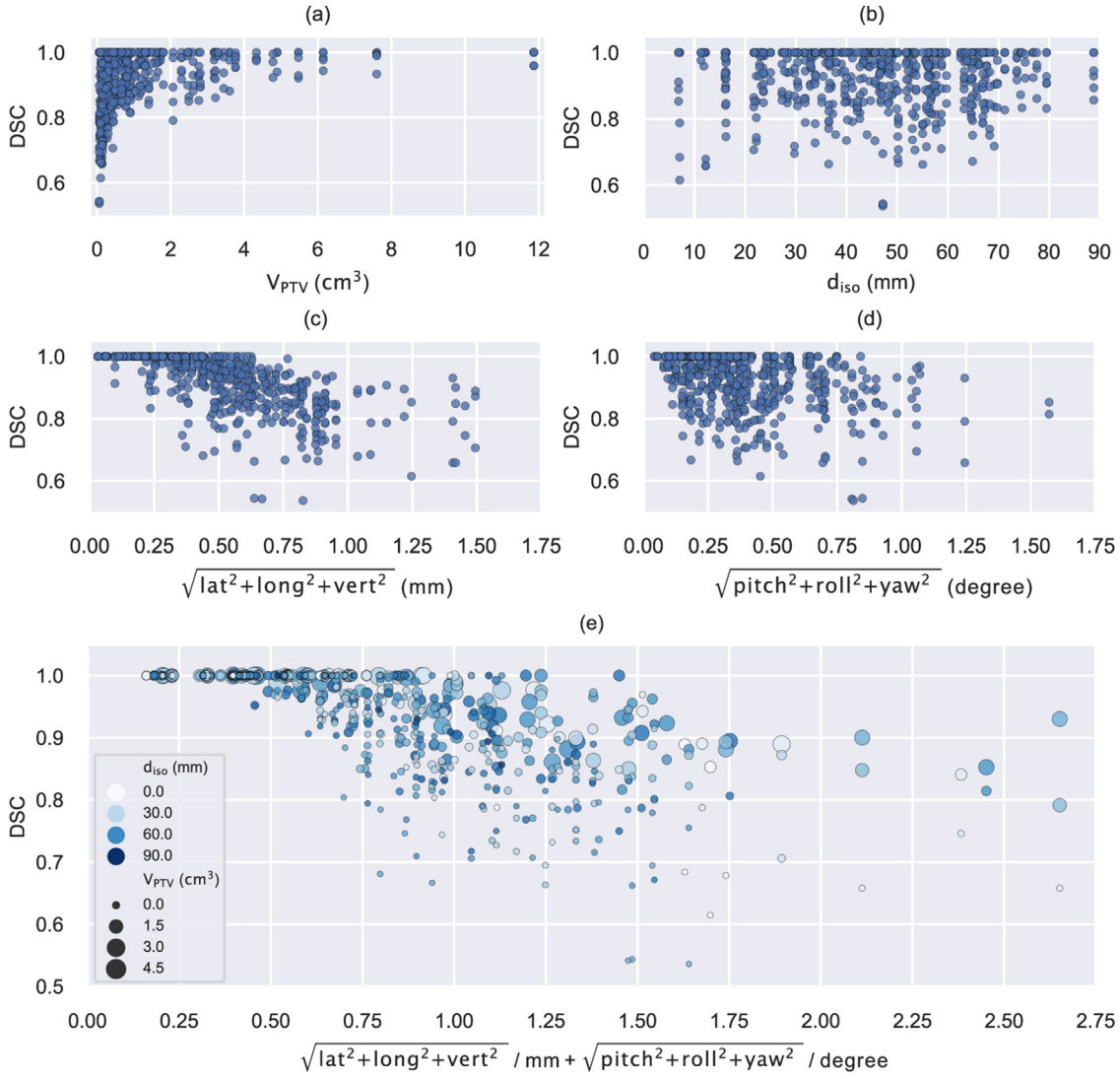

Figure 5. Correlation for 651 DSCs with geometrical properties such as PTV volume (a) and offset from the treatment isocenter (b) as well as with translational (c) and rotational patient misalignment (d) calculated for 130 PTVs. Panel (e) features 620 DSCs for 123 PTVs smaller than 4 cm^3 scattered against combined 6 DoF patient misalignment. The associated isocentric offset is color-coded, whereas the PTV volume is represented by the marker size.

Table 3
Ranking of the patients by decreasing geometrical risk of underdosage (i.e. ascending DSC). Each row represents the most unfavorable PTV and misalignment combination for its associated patient. The last row represents the patient with the largest DSC, i.e. at lowest geometrical risk of underdosage. DoF that are out of tolerance are in italics.

V_{PTV} (cm^3)	d_{iso} (mm)	Couch (°)	lat (mm)	long (mm)	vert (mm)	pitch (°)	roll (°)	yaw (°)	DSC
0.05	47.2	30	*0.8*	−0.2	0.3	*−0.7*	0.4	0.0	0.54
0.10	7.1	−40	*0.8*	*0.9*	0.3	0.1	0.1	0.4	0.61
0.13	12.2	10	*0.9*	*1.1*	−0.3	0.2	−0.2	*1.2*	0.66
0.13	36.5	60	0.6	−0.3	−0.5	0.3	0.1	−0.2	0.66
0.06	50.2	90	−0.1	*−0.8*	−0.1	0.1	0.0	−0.2	0.67
...									
0.66	11.9	−30	−0.1	0.3	−0.4	0.1	−0.3	0.1	0.96

Table 4
Overview of GTVs and PTVs for the worst-case patient. The table contains their volume and distance to the treatment isocenter. The original treatment plan was optimized such that each PTV was covered with a prescription isodose of 19 Gy at 98% of its volume.

	target volumes (TVs)				
	TV1	TV2	TV3	TV4	TV5
V_{GTV} (cm^3)	0.18	0.52	0.29	0.01	0.01
V_{PTV} (cm^3)	0.39	1.02	0.62	0.05	0.09
d_{iso} (mm)	42.1	56.1	39.7	47.2	55.1

Table 5
Statistical data for a few selected, relative treatment parameters assessed for the five PTVs of the worst-case patient. They were based on three distinct groups from pure translations, pure rotations and combinations of both. *N* represents the number of dose recalculations in each group, where values for all five treated PTVs are included.

	Group	*N*	min	max	Mean	SD
$\Delta D_{2\%}$ (Gy)	Translation	100	−3.3	0.2	−0.1	0.4
	Rotation	100	−0.4	0.1	0.0	0.1
	Combination	85	−2.2	0.1	−0.2	0.4
ΔD_{mean} (Gy)	Translation	100	−10.8	0.0	−1.5	1.8
	Rotation	100	−4.6	0.1	−0.6	0.9
	Combination	85	−7.6	−0.1	−2.4	1.9
$\Delta D_{98\%}$ (Gy)	translation	100	−13.7	−0.1	−4.5	3.2
	Rotation	100	−9.5	0.7	−2.4	2.3
	Combination	85	−12.0	0.0	−6.7	3.4
CCR (%)	Translation	100	0.5	98.0	27.4	22.6
	Rotation	100	−2.0	79.3	14.8	15.7
	Combination	85	1.3	92.0	38.3	21.0

smaller compared to the translational DoF. In addition, the combinations of translational and rotational misalignments were showing a similar trend in the relative $\Delta D_{98\%}$ parameter as indicated in Figure 6c. With the exception of PTV 5, the magnitude of combined systematic positioning errors was ranked in between pure translations and rotations. For PTV 5 however, the strong effects that pure translational positioning errors had on the $\Delta D_{98\%}$ tended to be suppressed by an interplay with rotational misalignments.

3.4 Dosimetric impact of clinical misalignments

For 20 patients, the comparison of relative DVH parameters for the two scenarios AC and NC is depicted for 75 PTVs and GTVs in Figure 7a and b, respectively.

Differences with respect to the treatment plan were more prominent in $D_{98\%}$ compared to $D_{2\%}$. In addition, the reported median values of the relative DVH parameters were lower in the NC scenario compared to the AC scenario. However, a substantial decrease of coverage, as reflected by the CCR parameter, was prominent in the NC scenario (Figure 7c). In particular, the parameter's 95% CI changed from 9.9% to 17.2% for the PTV and from 16.1% to 42.5% for the GTV, when analyzing the AC and NC scenario, respectively. The outcome of the statistical analysis is summarized in Table 6.

The influence of the geometrical PTV properties on CCR is visualized in Figure 8. The parameters were categorized based on the 33rd and 66th percentile of the corresponding range of volumes V_{PTV} and isocentric offsets d_{iso}. PTVs with a volume below 0.15 cm^3 were considered small and above 0.54 cm^3 they were classified as large structures. In between, structures were categorized as medium sized. Regarding the patient-specific distance to treatment isocenter, the PTVs were split in three groups of $d_{iso} < 39.7$ mm, $39.7\text{ mm} \leq d_{iso} \leq 53.8$ mm and $d_{iso} > 53.8$ mm and classified as near, medium ranged and far structures, respectively. For PTVs with a volume of $V_{PTV} > 2$ cm^3, the overall CCR difference between the plan and both misalignment scenarios was confined between −1.3% and 2.1%. The strongest outlier ($\Delta D_{98\%} = -3.6$ Gy and CCR = 30%) was detected in the NC scenario. It was associated to a very small PTV ($V_{PTV} = 0.05$ cm^3) treated at a medium ranged distance from the isocenter ($d_{iso} = 47.2$ mm).

4 Discussion

4.1 Analysis of patient misalignment

The studied misalignments in 6 DoF, reported by ET XV for 38 single-isocenter non-coplanar SRS patients with multiple brain metastases, revealed an accurate and precise ET-based setup in all DoF. The results from pre-positioning were compared to reported data from the literature and turned out to be similar [19,21,35,36]. The overall misalignment values after manual positioning were of relatively high magnitude. This

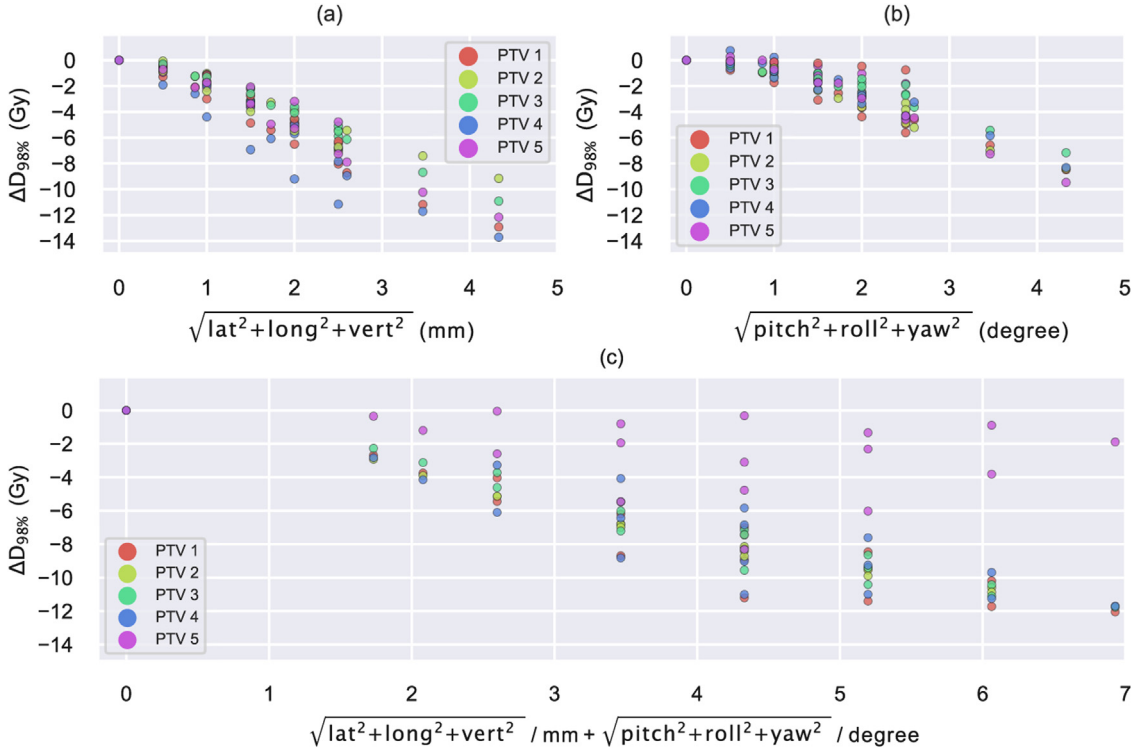

Figure 6. Scatterplot of $\Delta D_{98\%}$ against the corresponding DoF in pure translational (a), pure rotational (b), and combined misalignments (c). The five individual PTVs are color-coded.

Table 6
Reported p-values of Friedman (p_F) and Nemenyi test (p_{N_1}: Plan vs. AC, p_{N_2}: Plan vs. NC, p_{N_3}: AC vs. NC) for the associated treatment planning parameters. The tests were performed individually for each structure type, with a significance threshold $\alpha = 0.05 = 5\%$. The used data for PTVs, GTVs and OARs (brainstem, optic nerves, chiasm, hippocampus and the whole brain) consisted of 75, 75 and 130 entries per parameter and scenario, respectively.

	PTV				GTV				OAR			
	p_F	p_{N_1}	p_{N_2}	p_{N_3}	p_F	p_{N_1}	p_{N_2}	p_{N_3}	p_F	p_{N_1}	p_{N_2}	p_{N_3}
$D_{2\%}$	$<\alpha$	$<\alpha$	$<\alpha$	0.35	$<\alpha$	$<\alpha$	$<\alpha$	0.82	$<\alpha$	$<\alpha$	$<\alpha$	0.58
$D_{98\%}$	$<\alpha$	0.10	$<\alpha$	$<\alpha$	$<\alpha$	0.12	$<\alpha$	$<\alpha$	$<\alpha$	$<\alpha$	$<\alpha$	0.22
D_{mean}	$<\alpha$	$<\alpha$	$<\alpha$	$<\alpha$	$<\alpha$	$<\alpha$	$<\alpha$	$<\alpha$	0.67			
CCR	$<\alpha$	$<\alpha$	$<\alpha$	$<\alpha$	$<\alpha$	$<\alpha$	$<\alpha$	$<\alpha$				

was especially the case for translational DoF. It is assumed that these are linked to inconsistencies between X-ray-based positioning and preliminary laser-based patient alignment.

Institution-specific differences to our results are expected to be linked to imaging, immobilization and the used treatment couch to provide 6 DoF corrections. No systematic errors were reported for XVs at non-coplanar treatment couch angles, however the positioning precision was degraded due to random errors. Their source is most likely related to intra-fractional motion. It should be noted that a degradation of the positioning accuracy with time has been reported previously [37], along with the need to correct for intra-fractional positioning errors at different couch angles [19,38]. When delivering non-coplanar SRS without the possibility to correct the positioning errors at any given couch angle, this may put treatments with high numbers of MUs and many couch angles at an increased risk. Overall, the complete treatment workflow was determined to be appropriate in terms of geometric accuracy, as only around 22.5% of the acquired XVs at non-coplanar configurations were followed by a subsequent positioning correction. Other groups have reported even larger fractions, up to 2/3, which is indeed linked to different tolerance values (i.e. 0.5 mm and 0.5°) [19]. These smaller tolerance values may be exploited to further increase the accuracy. However, this comes with the price of an increased treatment time, as resulting from a possibly larger number of required positioning corrections.

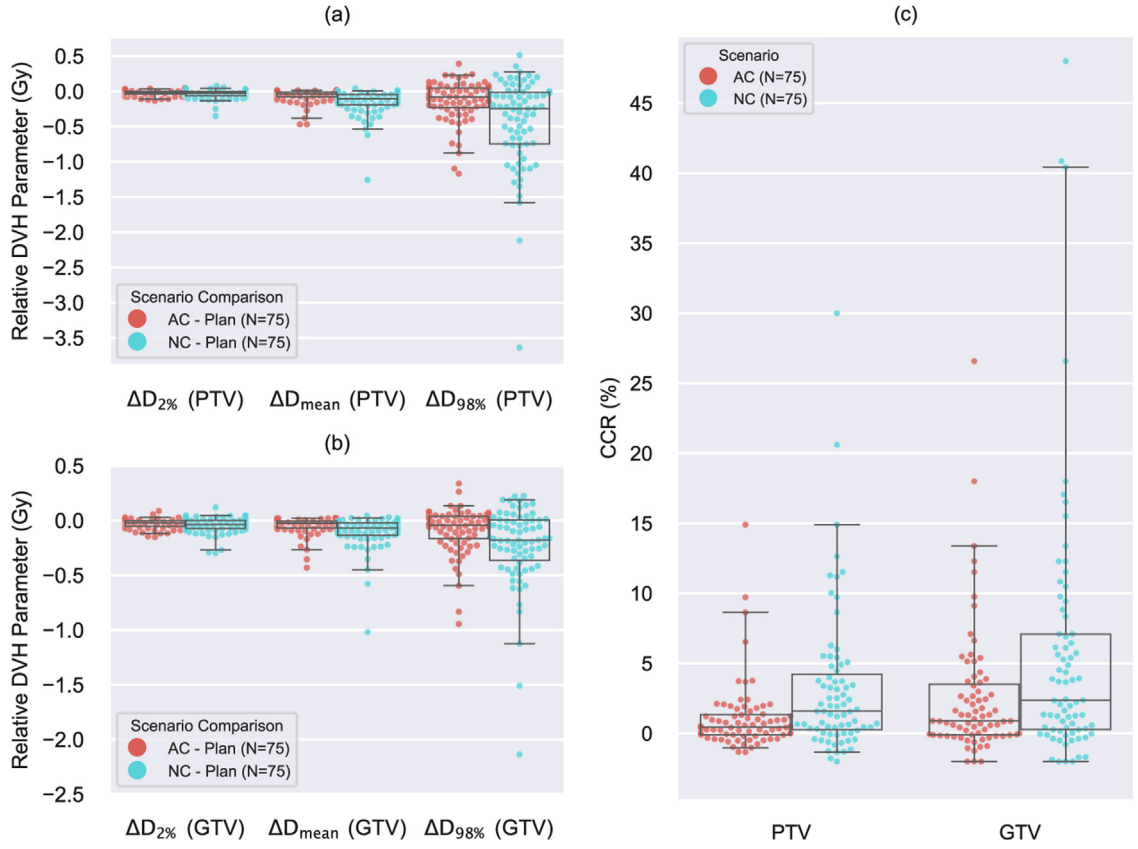

Figure 7. Relative DVH parameters for 75 PTVs (a), 75 GTVs (b) and CCR for both groups (c) at dose recalculation under AC and NC scenario. Positive CCR values reflect a loss of prescription isodose coverage in the given scenario compared to the treatment plan. The boxes span from the 25th percentile to the 75th percentile thus displaying the IQR. Their lower and upper whiskers indicate the range between the 2.5th percentile and 97.5th percentile. Values outside this 95% CI are considered outliers.

Translational offsets from the imaging isocenter were larger along the IS and RL directions than along the PA axis. This is in agreement with the fact that the directions perpendicular to the rotation axis are affected more strongly by inaccuracies in isocentric treatment couch rotation [20]. For the rotational DoF, the observed yaw misalignments are most probably the result from an interplay between these inaccuracies and residual patient motion. The increased pitch misalignments might be the result of weaker immobilization along the IS axis. It is expected that the rotational uncertainties may be alleviated by a combination of mask fixation and bite block system. However, this serves as a potential topic for further investigations.

4.2 Geometrical impact of patient misalignments

The DSC was chosen to estimate the risk of PTV underdosage geometrically, as it intrinsically incorporates the PTV's geometrical properties and the 6 DoF in patient misalignment. The risk assessment was based on DSC calculations performed for every patient, their corresponding PTVs and all related misalignments per couch angle individually. The smaller the DSC, the less the similarity between original and transformed structure and thus the higher the risk of a loss in the PTV coverage.

The calculated DSCs tended to diminish with decreasing PTV volume as apparent in Figure 5a. This is linked to the fact that small volumes are more sensitive to a misalignment, which determines a larger variation in DSC calculations. No special trend was detected for the isocentric offset d_{iso}, as seen in Figure 5b. Some PTVs which were close to the treatment isocenter still suffered from a higher risk of underdosage. The influence of overall misalignment in all 6 DoF on the DSC exhibits a general tendency of decreasing DSC with increasing misalignments, as visible in Figure 5c and d, as expected. As apparent in Figure 5e, negligible risk was reported for combined DoF up to 0.5, which corresponds to uniform misalignments about 0.15 mm and 0.15° in all directions. Such values are in fact comparable to the SDs found in this study for ET-based patient setup, as resulting from XSV values in Figure 3.

The assessment of the DSCs is a feasible procedure to estimate the patient-individual geometrical risk of PTV underdosage, before a dose recalculation has to be performed. However, the analysis of individual cases requires

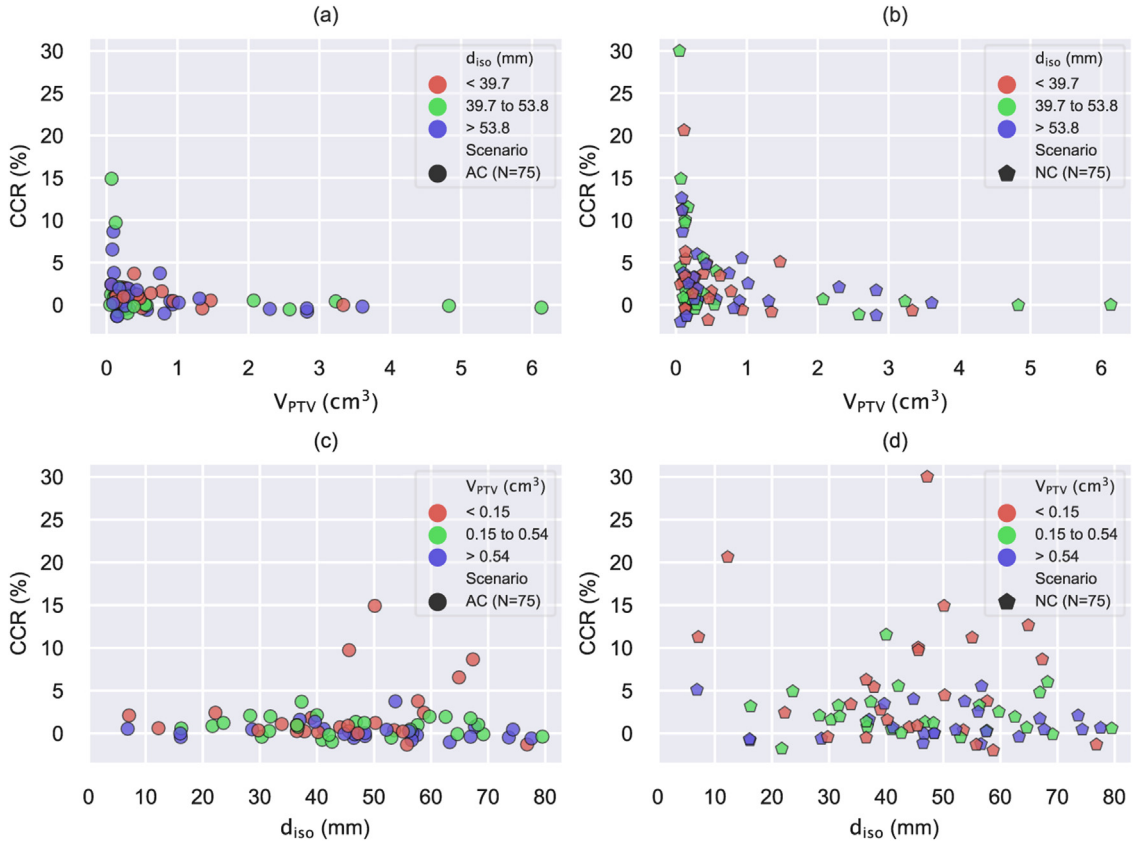

Figure 8. Relationship of CCR with geometrical PTV properties such as the absolute volume V_{PTV} or the offset from the treatment isocenter d_{iso} for both AC and NC scenarios. The respective property is categorized in three groups and color-coded.

the availability of detected misalignments during treatment. Therefore, such an analysis would be extremely valuable if performed online, but it cannot be used in the treatment planning stage to determine the potential risk for a given target structure. Alternatively, the risk might be estimated at the planning stage by using the ET XV's tolerance levels, that are used clinically to evaluate the positioning accuracy. Thus, a worst-case estimation can be made and potentially used to decide if a certain patient is feasible to be treated with single-isocenter SRS. As discussed later, combinations of individual DoF may also lead to significant dosimetric discrepancies, and should be therefore checked carefully.

4.3 Dosimetric impact of systematic misalignments

In our study, the dosimetric analysis was carried out relying on contrast-enhanced planning CTs, as used clinically at our institution. Although dosimetric effects can be expected for contrast injection, especially for small non-isocentric fields [39], this is counter-balanced by the advantage of better visibility of brain metastases in the treatment planning images [40]. In our specific study, the effects of systematic and clinical misalignments were investigated with treatment planning simulations on the same CT image. We can therefore expect that the highlighted relative differences would also apply to non-enhanced CTs.

From the data given in Table 5, a risk of compromised PTV coverage was detected for certain combinations of DoF. The magnitude of the translational and rotational misalignments plays a prominent role. In particular, an increase of the misalignments was causing a simultaneous reduction of the relative parameter $\Delta D_{98\%}$ as apparent in Figure 6. For the pure translational positioning errors, this is in agreement with what Guckenberger et al. [41] reported in terms of reduced PTV coverage for multiple-isocenter SRS. Accounting for both translational and rotational misalignments, no clear dependency on the distance to isocenter d_{iso} nor the PTV volume V_{PTV} was clearly highlighted, when considering the 5 different PTVs included in the worst case analysis (Figure 6). However, such a dependency was consistently reported in the literature [10–12,35]. It is expected that the restriction to a single patient is disadvantageous for such an analysis and a larger PTV cohort is required to reproduce the mentioned effects.

Nevertheless, reduced changes in $\Delta D_{98\%}$ were noted for PTV 5, when combinations of translational and rotational misalignments were studied (Figure 6c). Due to the PTV's classification as small ($V_{PTV} = 0.09\,cm^3$) and far away from the treatment isocenter ($d_{iso} = 55.1\,mm$), its corresponding relative

$\Delta D_{98\%}$ parameter was expected to be affected more strongly by the overall magnitude of the 6 DoF in patient misalignment.

As expected, a general trend of diminishing PTV coverage was detected for applied systematic misalignments of different magnitude in 6 DoF in a single patient study. It was observed that the interplay of the individual DoF might be of major importance for certain PTVs. The study could be enhanced by including more patients, orthogonal sampling of the DoF for each treatment couch angle and multiple PTV margins to gain further knowledge of collective effects. The acquired data may be helpful in relating the geometrical properties of metastases distributions to a risk of compromised coverage and thus be helpful to determine PTV-individual margins to account for that risk. The data might also serve as a basis to predict the most robust isocenter position for individual, single-isocenter treatments. In a long term outlook, such a study could rely on artificial neural networks, for example. This would require a large amount of data, especially in terms of dose recalculations, and therefore a higher degree of automatization in the presented recalculation workflow.

4.4 Dosimetric impact of clinical misalignments

The statistical analysis of the dosimetric impact of corrected and uncorrected patient misalignments revealed the strongest effects in the PTV coverage. Because high dose regions were still confined to the GTVs in both situations, no severe geographical misses were reported. This confirmed the adequacy of applied safety margins under the measured residual misalignments. Due to the lower PTV coverage in the NC vs. the AC scenario, lack of correction at non-coplanar angles leads to an increased risk of GTV underdosage for sources of uncertainties other than patient positioning (e.g. contouring and image fusion at treatment planning). For studying the loss of PTV coverage, no convincing dependency on the isocentric offsets was observed. As expected, small PTV volumes were linked to an increased risk of a reduced coverage. A statistical significant difference was found in $D_{98\%}$ between the treatment plan and its recalculation, if misalignments were not corrected. Conversely, if the positioning corrections were applied, the $D_{98\%}$ difference to the treatment plan was not considered significant. Therefore, it can be concluded that positioning verifications and corrections performed by ET are beneficial in achieving a PTV coverage close to what was initially planned. Alternatively, a dedicated isocenter may be used for lesion associated with a higher risk of underdosage. By this, the influence of rotational misalignments can be decreased appropriately. In the simulated AC scenario, residuals following couch corrections were assumed to be null, consistently with the fact that no XV was performed (i.e. residuals were unknown). Although this might potentially introduce heterogeneities in the AC scenario, we were able to observe a statistical significant difference among treatment planning, the AC and NC scenarios, with the AC scenario leading to better coverage. More specifically, even though we assumed null residuals when XV was not performed, we were still able to detect a significant difference between the AC scenario and the original treatment plan, which assumes perfect positioning. Therefore, the underlying assumption did not significantly alter the expected difference among the different scenarios, thus confirming the validity of our approach.

5 Conclusion

This study highlighted the important role of positioning verification and correction with ET at non-coplanar configurations in frameless single-isocenter SRS for patients with multiple brain metastases. Even though the depicted treatment workflow was verified to be suitable, the influence of intra-fractional motion on the treatment delivery should not be underestimated.

Uncorrected patient misalignments at non-coplanar treatment couch angles were linked to a significant loss of PTV coverage. The use of ET was found to have the potential to alleviate such effects to a certain degree. It is expected that exploring smaller tolerances for the system, additional MU or time-triggered acquisitions, various immobilization strategies and individually optimized PTV margins may even further enhance the accuracy and safety of frameless single-isocenter non-coplanar SRS treatments.

Ethical statement

This retrospective study was exempt from requiring ethics approval. Bavarian state law (Bayrisches Krankenhausgesetz/Bavarian Hospital Law §27 Absatz 4 Datenschutz/Dataprotection) allows the use of patient data for research, provided that any person's related data are kept anonymous. German radiation protection laws request a regular analysis of outcomes in the sense of quality control and assurance, thus in the case of purely retrospective studies no additional ethical approval is needed under German law.

Declaration of competing interests

The Department of Radiation Oncology of the University Hospital of LMU Munich holds research agreements with Brainlab, Elekta and ViewRay.

Acknowledgements

We want to thank our cooperation partners at Brainlab AG (Munich, Germany) namely Marc Göpfert, Wolfgang Ullrich and Thorsten Bschorr for providing a treatment planning system (TPS) prototype capable of incorporating patient misalignment into the dose recalculation process. We also like to thank Florian Kamp and the complete medical physics research team at the Department of Radiation Oncology of

the University Hospital of LMU Munich for their useful comments provided throughout this study.

References

[1] Schmitt D, Blanck O, Gauer T, Fix M, Brunner T, Fleckenstein J, et al. Technological quality requirements for stereotactic radiotherapy: expert review group consensus from the DGMP working group for physics and technology in stereotactic radiotherapy. Strahlenther Onkol 2020;196(5):421–43, http://dx.doi.org/10.1007/s00066-020-01583-2.

[2] Solberg TD, Boedeker KL, Fogg R, Selch MT, DeSalles AAF. Dynamic arc radiosurgery field shaping: a comparison with static field conformal and noncoplanar circular arcs. Int J Radiat Oncol Biol Phys 2001;49(5):1481–91, http://dx.doi.org/10.1016/S0360-3016(00)01537-6. URL: http://www.sciencedirect.com/science/article/pii/S0360301600015376.

[3] Clark GM, Popple RA, Young PE, Fiveash JB. Feasibility of single-isocenter volumetric modulated arc radiosurgery for treatment of multiple brain metastases. Int J Radiat Oncol Biol Phys 2010;76(1):296–302, http://dx.doi.org/10.1016/j.ijrobp.2009.05.029. URL: http://www.sciencedirect.com/science/article/pii/S0360301609007925.

[4] Huang Y, Chin K, Robbins JR, Kim J, Li H, Amro H, et al. Radiosurgery of multiple brain metastases with single-isocenter dynamic conformal arcs (SIDCA). Radiotherapy Oncol 2014;112(1):128–32, http://dx.doi.org/10.1016/j.radonc.2014.05.009. URL: http://www.sciencedirect.com/science/article/pii/S0167814014002394.

[5] Gevaert T, Steenbeke F, Pellegri L, Engels B, Christian N, Hoornaert M-T, et al. Evaluation of a dedicated brain metastases treatment planning optimization for radiosurgery: a new treatment paradigm? Radiat Oncol 2016;11, http://dx.doi.org/10.1186/s13014-016-0593-y. URL: https://www.ncbi.nlm.nih.gov/pmc/articles/PMC4736109/.

[6] Ruggieri R, Naccarato S, Mazzola R, Ricchetti F, Corradini S, Fiorentino A, et al. Linac-based VMAT radiosurgery for multiple brain lesions: comparison between a conventional multi-isocenter approach and a new dedicated mono-isocenter technique. Radiat Oncol 2018;13, http://dx.doi.org/10.1186/s13014-018-0985-2. URL: https://www.ncbi.nlm.nih.gov/pmc/articles/PMC5836328/.

[7] Hofmaier J, Bodensohn R, Garny S, Hadi I, Fleischmann DF, Eder M, et al. Single isocenter stereotactic radiosurgery for patients with multiple brain metastases: dosimetric comparison of VMAT and a dedicated DCAT planning tool. Radiat Oncol 2019;14, http://dx.doi.org/10.1186/s13014-019-1315-z. URL: https://www.ncbi.nlm.nih.gov/pmc/articles/PMC6560766/.

[8] Sahgal A, Ruschin M, Ma L, Verbakel W, Larson D, Brown PD. Stereotactic radiosurgery alone for multiple brain metastases? A review of clinical and technical issues. Neuro-Oncology 2017;19(Suppl. 2):ii2–15, http://dx.doi.org/10.1093/neuonc/nox001. URL: https://www.ncbi.nlm.nih.gov/pmc/articles/PMC5463499/.

[9] Hanna SA, Mancini A, Dal Col AH, Asso RN, Neves-Junior WFP. Frameless image-guided radiosurgery for multiple brain metastasis using VMAT: a review and an institutional experience. Front Oncol 2019;9, http://dx.doi.org/10.3389/fonc.2019.00703. URL: https://www.ncbi.nlm.nih.gov/pmc/articles/PMC6693418/.

[10] Clark GM, Fiveash JB, Prendergast BM, Willey CW, Spencer SA, Thomas EM, et al. Dosimetric impact of patient rotational setup errors with frameless single-isocenter, multi-target volumetric modulated arc radiosurgery for multiple brain metastases. Int J Radiat Oncol Biol Phys 2011;81(2 Suppl.):S888, http://dx.doi.org/10.1016/j.ijrobp.2011.06.1590. URL: http://www.sciencedirect.com/science/article/pii/S0360301611024114.

[11] Roper J, Chanyavanich V, Betzel G, Switchenko J, Dhabaan A. Single-isocenter multiple-target stereotactic radiosurgery: risk of compromised coverage. Int J Radiat Oncol Biol Phys 2015;93(3):540–6, http://dx.doi.org/10.1016/j.ijrobp.2015.07.2262. URL: http://www.sciencedirect.com/science/article/pii/S0360301615030126.

[12] Selvan KT, Padma G, Revathy MK, Nambi Raj NA, Senthilnathan K, Babu PR. Dosimetric effect of rotational setup errors in single-isocenter volumetric-modulated arc therapy of multiple brain metastases. J Med Phys 2019;44(2):84–90, http://dx.doi.org/10.4103/jmp.JMP_103_18. URL: https://www.ncbi.nlm.nih.gov/pmc/articles/PMC6580820/.

[13] Smith K, Balter P, Duhon J, White GA, Vassy DL, Miller RA, et al. AAPM medical physics practice guideline 8.a.: linear accelerator performance tests. J Appl Clin Med Phys 2017;18(4):23–39, http://dx.doi.org/10.1002/acm2.12080.

[14] Li G, Ballangrud A, Kuo LC, Kang H, Kirov A, Lovelock M, et al. Motion monitoring for cranial frameless stereotactic radiosurgery using video-based three-dimensional optical surface imaging. Med Phys 2011;38(7):3981–94, http://dx.doi.org/10.1118/1.3596526.

[15] Pan H, Cerviño LI, Pawlicki T, Jiang SB, Alksne J, Detorie N, Russell M, Carter BS, Murphy KT, et al. Frameless, real-time, surface imaging-guided radiosurgery clinical outcomes for brain metastases. Neurosurgery 2012;71(4):844–52, http://dx.doi.org/10.1227/NEU.0b013e3182647ad5. URL: http://academic.oup.com/neurosurgery/article/71/4/844/2594039.

[16] Zollner B, Heinz C, Pitzler S, Manapov F, Kantz S, Rottler MC, et al. Stereoscopic X-ray imaging, cone beam CT, and couch positioning in stereotactic radiotherapy of intracranial tumors: preliminary results from a cross-modality pilot installation. Radiat Oncol 2016;11, http://dx.doi.org/10.1186/s13014-016-0735-2. URL: https://www.ncbi.nlm.nih.gov/pmc/articles/PMC5142336/.

[17] Schmidhalter D, Malthaner M, Born EJ, Pica A, Schmueckking M, Aebersold DM, et al. Assessment of patient setup errors in IGRT in combination with a six degrees of freedom couch. Z Med Phys 2014;24(2):112–22, http://dx.doi.org/10.1016/j.zemedi.2013.11.002. URL: http://www.sciencedirect.com/science/article/pii/S0939388913001359.

[18] Wiant D, Liu H, Hayes TL, Shang Q, Mutic S, Sintay B. Direct comparison between surface imaging and orthogonal radiographic imaging for SRS localization in phantom. J Appl Clin Med Phys 2018;20(1):137–44, http://dx.doi.org/10.1002/acm2.12498. URL: https://www.ncbi.nlm.nih.gov/pmc/articles/PMC6333181/.

[19] Grohmann M, Todorovic M, Petersen C. Der einfluss von intrafraktioneller patientenbewegung auf die behandlungsgenauigkeit bei radiochirurgie multipler hirnmetastasen. Strahlenther Onkol 2021;197(Suppl 1):S51–2, http://dx.doi.org/10.1007/s00066-021-01791-4.

[20] Ackerly T, Lancaster CM, Geso M, Roxby KJ. Clinical accuracy of ExacTrac intracranial frameless stereotactic system. Med Phys 2011;38(9):5040–8, http://dx.doi.org/10.1118/1.3611044.

[21] Badakhshi H, Kaul D, Wust P, Wiener E, Buadch V, Graf R. Image-guided stereotactic radiosurgery for cranial lesions: large margins compensate for reduced image guidance frequency. Anticancer Res 2013;33(10):4639–43. URL: http://ar.iiarjournals.org/content/33/10/4639.

[22] Koubuchi S, Takakura T, Nakamura M, Mizowaki T, Nakata M, Hiraoka M. Accuracy of positional correction for the floor-mounted kV X-ray IGRT system in angled couch positions. Radiol Phys Technol 2014;7(2):373–8, http://dx.doi.org/10.1007/s12194-014-0275-0.

[23] Ma J, Chang Z, Wang Z, Jackie Wu Q, Kirkpatrick JP, Yin F-F. ExacTrac X-ray 6 degree-of-freedom image-guidance for intracranial non-invasive stereotactic radiotherapy: comparison with kilovoltage cone-beam CT. Radiotherapy Oncol 2009;93(3):602–8, http://dx.doi.org/10.1016/j.radonc.2009.09.009. URL: http://www.sciencedirect.com/science/article/pii/S016781400900557X.

[24] Murphy MJ, Balter J, Balter S, BenComo JA, Das IJ, Jiang SB, et al. The management of imaging dose during image-guided radiotherapy: report of the AAPM task group 75: imaging dose during image-guided radiotherapy. Med Phys 2007;34(10):4041–63, http://dx.doi.org/10.1118/1.2775667.

[25] Tanaka Y, Oita M, Inomata S, Fuse T, Akino Y, Shimomura K. Impact of patient positioning uncertainty in noncoplanar intracranial stereotactic radiotherapy. J Appl Clin Med Phys 2020;21(2):89–97, http://dx.doi.org/10.1002/acm2.12820.
[26] Kocher M, Wittig A, Piroth MD, Treuer H, Seegenschmiedt H, Ruge M, et al. Stereotactic radiosurgery for treatment of brain metastases. Strahlentherapie Onkol 2014;190(6):521–32, http://dx.doi.org/10.1007/s00066-014-0648-7.
[27] Soffietti R, Abacioglu U, Baumert B, Combs SE, Kinhult S, Kros JM, et al. Diagnosis and treatment of brain metastases from solid tumors: guidelines from the European Association of Neuro-Oncology (EANO). Neuro-Oncology 2017;19(2):162–74, http://dx.doi.org/10.1093/neuonc/now241. URL: https://www.ncbi.nlm.nih.gov/pmc/articles/PMC5620494/.
[28] Sharp G, Li R, Wolfgang J, Chen G, Peroni M, Spadea M, et al. Plastimatch – an open source software suite for radiotherapy image processing. In: XVI'th international conference on the use of computers in radiotherapy (ICCR). 2010.
[29] Dice LR. Measures of the Amount of Ecologic Association Between Species. Ecology 1945;26(3):297–302, http://dx.doi.org/10.2307/1932409.
[30] Sørenson T. A method of establishing groups of equal amplitude in plant sociology based on similarity of species content and its application to analyses of the vegetation on Danish commons, vol. 5. 4th ed. Kongelige Danske Videnskabernes Selskab; 1948.
[31] Friedman M. The use of ranks to avoid the assumption of normality implicit in the analysis of variance. J Am Statis Assoc 1937;32(200):675–701, http://dx.doi.org/10.1080/01621459.1937.10503522.
[32] Nemenyi, P. Distribution-free multiple comparisons. PhD Thesis, Princeton University; 1963.
[33] Demšar J. Statistical comparisons of classifiers over multiple data sets. J Mach Learn Res 2006;7:1–30. URL: http://www.jmlr.org/papers/v7/demsar06a.html.
[34] Kendall MG, Gibbons JD. Rank correlation methods. 5th ed. Edward Arnold, London: Charles Griffin Book; 1990.
[35] Jin H, Keeling VP, Ali I, Ahmad S. Dosimetric effects of positioning shifts using 6D-frameless stereotactic Brainlab system in hypofractionated intracranial radiotherapy. J Appl Clin Med Phys 2016;17(1):102–11, http://dx.doi.org/10.1120/jacmp.v17i1.5682. URL: https://www.ncbi.nlm.nih.gov/pmc/articles/PMC5690222/.
[36] Keeling V, Hossain S, Jin H, Algan O, Ahmad S, Ali I. Quantitative evaluation of patient setup uncertainty of stereotactic radiotherapy with the frameless 6D ExacTrac system using statistical modeling. J Appl Clin Med Phys 2016;17(3):111–27, http://dx.doi.org/10.1120/jacmp.v17i3.5959.
[37] Hoogeman MS, Nuyttens JJ, Levendag PC, Heijmen BJM. Time dependence of intrafraction patient motion assessed by repeat stereoscopic imaging. Int J Radiat Oncol Biol Phys 2008;70(2):609–18, http://dx.doi.org/10.1016/j.ijrobp.2007.08.066. URL: http://www.sciencedirect.com/science/article/pii/S0360301607041491.
[38] Barnes M, Yeo A, Thompson K, Phillips C, Kron T, Hardcastle N. A retrospective analysis of setup and intrafraction positional variation in stereotactic radiotherapy treatments. J Appl Clin Med Phys 2020;21(12):109–19, http://dx.doi.org/10.1002/acm2.13076.
[39] Kim HJ, Chang AR, Park Y-K, Ye S-J. Dosimetric effect of CT contrast agent in CyberKnife treatment plans. Radiat Oncol 2013;8(1):244, http://dx.doi.org/10.1186/1748-717X-8-244.
[40] Hartgerink D, Swinnen A, Roberge D, Nichol A, Zygmanski P, Yin F-F, et al. LINAC based stereotactic radiosurgery for multiple brain metastases: guidance for clinical implementation. Acta Oncol 2019;58(9):1275–82, http://dx.doi.org/10.1080/0284186X.2019.1633016.
[41] Guckenberger M, Roesch J, Baier K, Sweeney RA, Flentje M. Dosimetric consequences of translational and rotational errors in frame-less image-guided radiosurgery. Radiat Oncol 2012;7, http://dx.doi.org/10.1186/1748-717X-7-63. URL: http://www.ncbi.nlm.nih.gov/pmc/articles/PMC3441228/.